Journal of Ionic Liquids xxx (xxxx) 100018

Contents lists available at ScienceDirect

Journal of Ionic Liquids

journal homepage: www.elsevier.com

Journal Cover Image

CO_2-driven surface reconstruction in quaternary ammonium ionic liquid-propanol solutions

Hiroshi Abe *, Hiroaki Kishimura

Department of Materials Science and Engineering, National Defense Academy, Yokosuka 239-8686, Japan

ARTICLE INFO

Keywords:
Quaternary ammonium ionic liquids
X-ray reflectivity
Surface reconstruction
Specific surface layering
CO_2 capture

ABSTRACT

X-ray reflectivity (XRR) examined surface structures of hydrophobic quaternary ammonium ionic liquids, and their propanol mixtures were examined by XRR. The quaternary ammonium cations were $[N(n)111]^+$ (n = 3, 4, and 6) and an anion was commonly bis(trifluoromethanesulfonyl)imide, $[TFSI]^-$. The surface tension of pure [N(n)111][TFSI] increased with increasing n. Pure [N(n)111][TFSI] surface structures were stable in all gas atmospheres. The XRR of [N3111][TFSI]-1-propanol equilibrated showed CO_2-induced surface roughness. Time-resolved XRR under CO_2 of [N(n)111][TFSI]-propanol provided surface instabilities and a reconstruction process. The addition of 2-propanol to CO_2 in [N4111][TFSI] promoted specific surface layering and a large amount of CO_2 capture.

1. Introduction

CO_2 emissions have been a major contributor to global warming of the Earth's surface and atmosphere. Carbon capture and storage (CCS) is one solution to problems (Rosa et al., 2020). In addition to CCS, CO_2 capture and utilization (CCU) technology is being proposed, with utilization and removal pathways taken into account (Schoedel et al., 2016). When combined with energy, CCS and CCU form a carbon-neutral energy system (Hepburn et al., 2019). The urgent challenges for a climate problem have been ongoing on the molecular level. Ionic liquids (ILs), which are simple molecules, are a candidate for CO_2 capture. Due to the nearly zero vapor pressure of the ILs, the ILs are easily recycled. It was reported that the high physical sorption of CO_2 is realized by 1-butyl-3-methylimidazolium hexafluorophosphate, $[C_4mim][PF_6]$ (Blanchard et al., 1999). Under high temperature and high pressure, a lot of supercritical CO_2 ($scCO_2$) were absorbed into $[C_4mim][PF_6]$. The $scCO_2$ absorption properties were expressed in the *P-T* phase diagram. In CO_2 capture studies, the $scCO_2$ capture system was mainly optimized (Bara et al., 2009). High $scCO_2$ capture was obtained by bis(trifluoromethanesulfonyl)imide, $[TFSI]^-$, anion. Moreover, it was pointed out that gas selectivity is also important for industrial applications (Bara et al., 2009). CO_2 capture using ILs has been summarized in the literature (Brennecke and Gurkan, 2010; Ramdin et al., 2012; Zeng et al., 2017). Based on implications for process design, the cost for $scCO_2$ capture using the ILs was evaluated precisely (Zhai and Rubin, 2017; Mota-Martinez et al., 2018). Using polymerized ILs, normal CO_2 (nCO_2) is captured at ambient pressure and temperature (Tang et al., 2005). The reversible sorption and desorption of nCO_2 were monitored at room temperature. For further cost-cutting, nCO_2 capture using propanol-diluted quaternary ammonium ILs was examined (Abe et al., 2016). *N*-trimethyl-*N*-butylammonium bis(trifluoromethanesulfonyl)imide, [N4111][TFSI], -2-propanol indicates the highest nCO_2 capture. Since the ILs are expensive, the propanol dilution contributes to the cost cutting. To probe nCO_2 in the mixtures, the quaternary ammonium IL-propanol mixtures were quenched into liquid nitrogen (Abe et al., 2020). nCO_2 capture using the propanol-diluted ILs without pressing and heating devices is a promising system for cost-cutting and downsizing purposes. Very recently, a series of quaternary ammonium cations with tetrafluoroborate anion was examined for CO_2 capture (Su et al., 2021). Density functional theory calculations indicated a geometrical relation between the ILs and CO_2.

The surface structures of ILs are quite different from the bulk structures. Surface structures of 1-alkyl-3-methylimidazolium, $[C_nmim]^+$, were determined by X-ray reflectivity (XRR), where n reveals the alkyl chain length of the $[C_nmim]^+$ cations (Carmichael et al., 2001; Solutskin et al., 2005, 2006; Mezgera et al., 2013). From the surface-normal electron densities, models of the surface structures of the ILs were proposed. Molecular dynamics simulations confirmed the surface layering of the ILs (Yan et al., 2006; Shimizu et al., 2018). Furthermore, surface structures had a relationship with surface tensions, with surface tensions being inversely proportional to the alkyl chain length of the $[C_nmim]^+$ cations. Under an electric field, the *in-situ* observation of the

* Corresponding author.
E-mail address: ab@nda.ac.jp (H. Abe).

https://doi.org/10.1016/j.jil.2022.100018
Received 1 December 2021; Received in revised form 12 January 2022; Accepted 15 January 2022

electric double layer (EDL) of 1-butyl-1-methylpyrrolidinium bis(trifluoromethanesulfonyl)imide, [C_4mpyr][TFSI], was carried out by neutron reflectivity (NR) (Lauw et al., 2012). A relationship between EDL formation and the electrochemical properties was carried. Using XRR and NR in conjunction can extract the hidden information about complex surface structures of quaternary ammonium IL-propanol solutions relating to $n$$CO_2$ capture (Abe et al., 2020). Under the $n$$CO_2$ condition, specific surface layering of [N4111][TFSI]-2-propanol occurred. The surface structure aided in the increased efficiency of $n$$CO_2$ capture.

In this study, using XRR, surface structures of [N(n)111][TFSI] (n = 3, 4, and 6) were examined by changing propanol concentrations, propanol isomers, and gas circumstances. In pure [N(n)111][TFSI], time-invariant and stable surfaces were formed at any type of gases. Kinetic behaviors of the [N(n)111][TFSI]-propanol solutions were observed by time-resolved XRR. During an early stage of $n$$CO_2$ absorption, kinetic surface reconstructions by $n$$CO_2$ were observed.

2. Materials and methods

The quaternary ammonium cations were *N,N,N*-trimethyl-*N*-propyl ammonium ([N3111]$^+$), [N4111]$^+$, and *N*-hexyl-*N,N,N*-trimethylammonium ([N6111]$^+$) (Kanto Chemical Co., Sigma-Aldrich Co., and Solvionic Co.) The molecular structures of the ILs are shown in Fig. 1. For each gas flowing experiments, [N3111][TFSI]-x mol% 1- and 2-propanol (x = 20, 40, 60, and 75 mol%) were prepared. In the case of the [N4111][TFSI]-based mixtures, 75 mol% 1- and 2-propanol mixtures were utilized. 20, 40, 60, and 70 mol% 1- and 2-propanol were added into [N6111][TFSI]. Hydrophobic ILs featuring the [TFSI]$^-$ anion were used in this study to prevent water contamination from atmospheric moisture. The [TFSI]$^-$ anion has two stable conformers: one is *cis* (C_1), and the other is *trans* (C_2) (Fig. 1). The conformational ratio of C_1 and C_2 had the amount of $n$$CO_2$ capture in [N4111][TFSI]-propanol solutions (Abe et al., 2016). The additives 1-propanol and 2-propanol (Kanto Chem. Co.) were also used.

The XRR measurements were carried out using a SmartLab (Rigaku Co.). An incident wavelength λ, of 1.54054 Å (Cu Kα_1) was obtained by a Ge(220) double monochromator. The X-ray windows of a gas replacement container were Kapton films, with a thickness of 7.5 μm. Inside the container, temperature was fixed at 23 °C within 0.5 °C. A free liquid surface, whose size is 60 × 30 mm^2, was obtained on the Teflon plate. The air was replaced with He, N_2, or CO_2 by flowing the gas through for 20 mL/min during the sample position adjustment for 3–5 min. After the adjustment, a gas supply was stopped, and time-resolved XRR measurements started. The scattered wavevector, Q, was provided as $Q = 4\pi(\sin\theta)/\lambda$ (Å^{-1}).

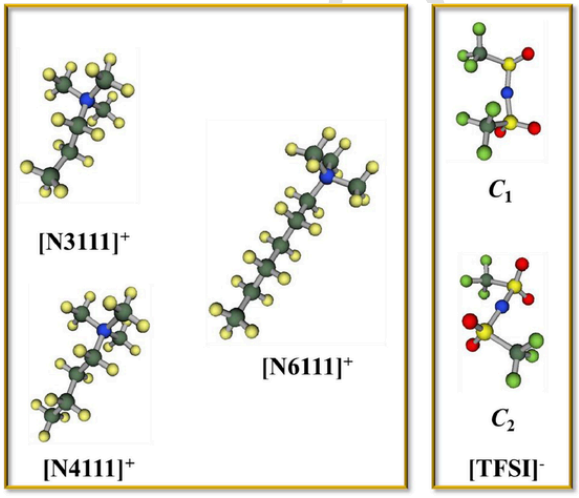

Fig. 1. Molecular structures of quaternary ammonium ionic liquids.

Surface tension was measured using the capillary rise method (Dyne Gauge, DG-1, Surfgauge Instruments Co.) (Abe et al., 2018; Nemoto et al., 2021). The surface tension was obtained using the bulk densities (ρ_{bulk}) as listed in Table 1 (Matsumoto et al., 2000; Zhang et al., 2006). The measurement range was 0–80 mN/m and its resolution was 1 mN/m.

To monitor propanol in the mixture during CO_2 flowing, time-resolved Raman spectra were measured in a backscattering geometry using a micro-Raman spectrometer (RA-07F, Seishin-Shoji) equipped with a monochromator (500M, Horiba Jobin Yvon) and a charge-coupled device detector (Symphony, Horiba Jobin Yvon). Radiation of 532 nm from a Nd:YAG laser was used as an excitation source with a power of 20mW. The Raman spectra were measured at room temperature and ambient pressure, and CO_2 flowing rate was 20mL/mim. Fig. S1 reveals time dependence of Raman spectra of [N4111][TFSI]-80 mol% 1-propanol (Fig. S1). The Raman band of 1-propanol appeared additionally at around 860 cm^{-1} (Abe et al., 2020), which indicated by the blue arrow (Fig. S1). Even under CO_2 flowing for 5 min, 1-propanol did not change

3. Results and discussion

3.1. Stable surface structures of pure quaternary ammonium ionic liquids

Surface tensions of pure [N(n)111][TFSI] (n = 3, 4, and 6) were measured at room temperature using ρ_{bulk} (Table 1). In contrast to [$C_n$mim][TFSI] (Shimizu et al., 2018), surface tensions of pure [N(n)1111][TFSI] increased proportionally to n. Since an anion is common in both systems, the surface tensions are originated from the cation behaviors near the surface. At least, the surface state of [N(n)111][TFSI] could differ from that of [$C_n$mim][TFSI].

The surface structure of pure [N4111][TFSI] was investigated at room temperature. Fig. 2 indicates the equilibrated XRR of pure [N4111][TFSI] under air, He, N_2, or CO_2. XRR coincided with any gas circumstances. The types of gases did not modify XRR. This tendency also appeared in pure [N3111][TFSI], and [N6111][TFSI]. More inter-

Table 1
Surface tensions and bulk densities and of pure quaternary ammonium ionic liquids, [N(n)111][TFSI].

		[N3111][TFSI]		[N4111][TFSI]		[N6111][TFSI]	
Surface tension [mN/m]	σ	18.6		20.4		22.7	
Density [g/cm3]	ρbulk	1.44	Matsumoto et al. (2000)	1.41	Zhang et al. (2006)	1.33	Zhang et al. (2006)

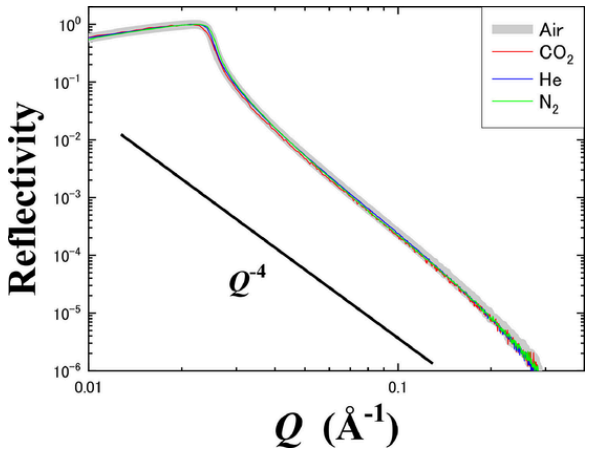

Fig. 2. X-ray reflectivity (XRR) of pure [N4111][TFSI]. Thick gray curve indicates equilibrated XRR under the air.

estingly, only under the He circumstance, many bubbles were formed on the bottom of the Teflon plate except for pure [N6111][TFSI]. For instance, the bubbles of pure [N4111][TFSI] are shown in Fig. 3. Compared with CO_2, He solubility in the ionic liquids was quite low (Chau et al., 2013). To investigate gas-driven surface changes, the time dependence of XRR of pure [N4111][TFSI] in air or CO_2 was measured (Fig. 4). The XRR of pure [N4111][TFSI] was time-invariant, and other ILs also provided time-invariant XRR under all gas conditions. As a result, in pure [N(n)111][TFSI], the stable surface was formed in the presence of air, He, N_2, or CO_2. In the gas selectivity experiment (Abe et al., 2016), [N4111][TFSI]-propanol absorbed very little N_2. It is deduced that N_2 could be repulsive to [N4111][TFSI] on the surface. Thus, under N_2, no bubbles were formed in any [N(n)111][TFSI]-propanol.

The refractive index of X-rays, n_r, is provided by (Veldhuis et al., 2014),

$$n_r = 1 - -d - -ib \tag{1}$$

where $\delta = \lambda^2 r_e \rho_e/2\pi$, $\beta = \lambda\mu/4\pi$: r_e the classical electron radius (2.818×10^{-5} Å), ρ_e the electron density, and μ the attenuation coefficient. Under very small angles, the critical angle (θ_c) is approximated as (Veldhuis et al., 2014),

$$\theta_c \approx \sqrt{2\delta} = \sqrt{\frac{\lambda^2 r_e \rho_e}{\pi}}. \tag{2}$$

On the other hand, mass density (ρ_m) is obtained by,

$$\rho_m = \frac{\rho_e M}{N_A Z}. \tag{3}$$

Here, N_A indicates Avogadro's number. The molecular weight and a total number of electrons are expressed by M and Z, respectively. Using Eqs. (2) and (3), ρ_m is directly connected with θ_c as follows;

$$\theta_c = \sqrt{\frac{\lambda^2 r_e N_A Z}{\pi M}\rho_m}. \tag{4}$$

In addition to the surface intensity, the XRR profile is significant. If the critical wavevector ($Q_c = 4\pi\sin(\theta_c)/\lambda$) is introduced, reflectivity is given approximately by $\left(\frac{Q_c}{2Q}\right)^4$ satisfying with $Q_c \ll Q$ (Tidswell et al., 1990). However, liquid free surface fluctuates naturally, and surface roughness is not ignored. For instance, the roughness of pure water was estimated by introducing the root-mean-square roughness, which obeys Gaussian statistics (Braslau et al., 1985). The observed rapid decay of XRR on the Q scale means that the surface roughness in the liquid state is an intrinsic property. If the surface roughness is predominant, intensity dumping becomes more remarkable. In case of pure [N4111][TFSI], the observed XRR did not obey the Q^{-4} law (Fig. 2). The surface state of pure [N(n)111][TFSI] is not described as the ideal flatness.

Fig. 3. Helium bubbles on the bottom in pure [N4111][TFSI]. Only under the helium circumstance, the bubbles appeared except for pure [N6111][TFSI].

The dynamic property of surface structure is important for gas absorption (Naeiji et al., 2020). In general, it is predicted that the gas atmosphere directly influences the surface state of the ILs. As a result, the time dependence of XRR was determined by varying He, N_2, or CO_2. To investigate gas-driven surface changes, the time dependence of XRR of pure [N4111][TFSI] in air or CO_2 was measured (Fig. 4). The XRR of pure [N4111][TFSI] was time-invariant, and other ILs also provided time-invariant XRR under all gas conditions. As a result, in pure [N(n)111][TFSI], the stable surface was formed in the presence of air, He, N_2, or CO_2.

3.2. Equilibrated surface structures in quaternary ammonium ionic liquid-propanol solutions

Fig. 5 shows equilibrated XRR of [N3111][TFSI]-x mol% propanol. From Eq. (4), $\theta_c \propto \sqrt{\rho_m}$ is obtained. Since the critical angle (θ_c) is quite small, $\sin(\theta_c)$ is approximated to be θ_c. Therefore, Eq. (4) is transformed to,

$$Q_c \propto \sqrt{\rho_m} \tag{5}$$

Q_c shifting by CO_2 is connected with the surface density change, $\Delta\rho_m$, using Eq. (5). To clarify the surface influence by CO_2 (Abe et al., 2020), $\Delta\rho_m$ is defined as,

$$Dr_m = r_{CO2} - r_{air} \tag{6}$$

Simultaneously, as another indicator of Q_c for mixing effect, Q_c (pure) of pure [N(n)111][TFSI] is used as a reference. Then, Q_c shifting, ΔQ_c, is provided by,

$$\Delta DQ_c = Q_c\,(\text{mix}) - -Q_c\,(\text{pure}) \tag{7}$$

In both of [N3111][TFSI]-20.0 mol% 1- and 2-propanol mixtures, XRR of the mixtures almost coincided with XRR of pure [N3111][TFSI], expressed by the thick gray curve (Fig. 5). For simplicity, XRR(IL, x, i, gas) is described using types of ILs (N3, N4, N6, and D), concentration (x mol%), i-propanol ($i = 1$ or 2), and the gas circumstance. N3, N4, and N6 reveal [N3111][TFSI], [N4111][TFSI], and [N6111][TFSI], respectively. The propanol additives below 20 mol% did not influence the surface structures in the mixed system. This result contradicted with the [N4111][TFSI]-propanol system (Abe et al., 2020). With increasing the propanol concentration, drastic propanol isomer effect appeared in XRR(N3, 40, 1, air) and XRR(N3, 40, 2, air) (Fig. 5). From the Q_c positions of the 40 mol% 1-propanol mixture, the surface density increased a little by CO_2 ($0 < \Delta\rho_m$). In the 40 mol% 2-propanol mixture, Q_c did not change ($\Delta\rho_m = 0$). CO_2-driven surface enrichment occurred in the 40 mol% 1-propanol mixture. Moreover, the intensity dumping of XRR (N3, 40, 1, CO_2) reflected large surface roughness. The propanol isomer effect of the 40 mol% mixtures is explained by simultaneous surface enrichment and roughness by CO_2. In XRR(N3, 60, 1, CO_2), the above tendency is much enhanced. Consequently, by CO_2, the surface roughness increased extensively at around 40-60 mol% 1-propanol. In the quenched bulk of [N3111][TFSI]-1-propanol mixtures (Abe et al., 2020), the 1-propanol Raman band decreased a lot by CO_2. Therefore, both at surface and bulk states of [N3111][TFSI]-1 propanol, CO_2 could disturb the network among cation, anion, and 1-propanol. However, the 2-propanol-based system indicated no CO_2-induced XRR dumping (Fig. 5). The non-CO_2 influence was also seen in the quenched bulk state of [N3111][TFSI]-2-propanol (Abe et al., 2020). No CO_2-induced

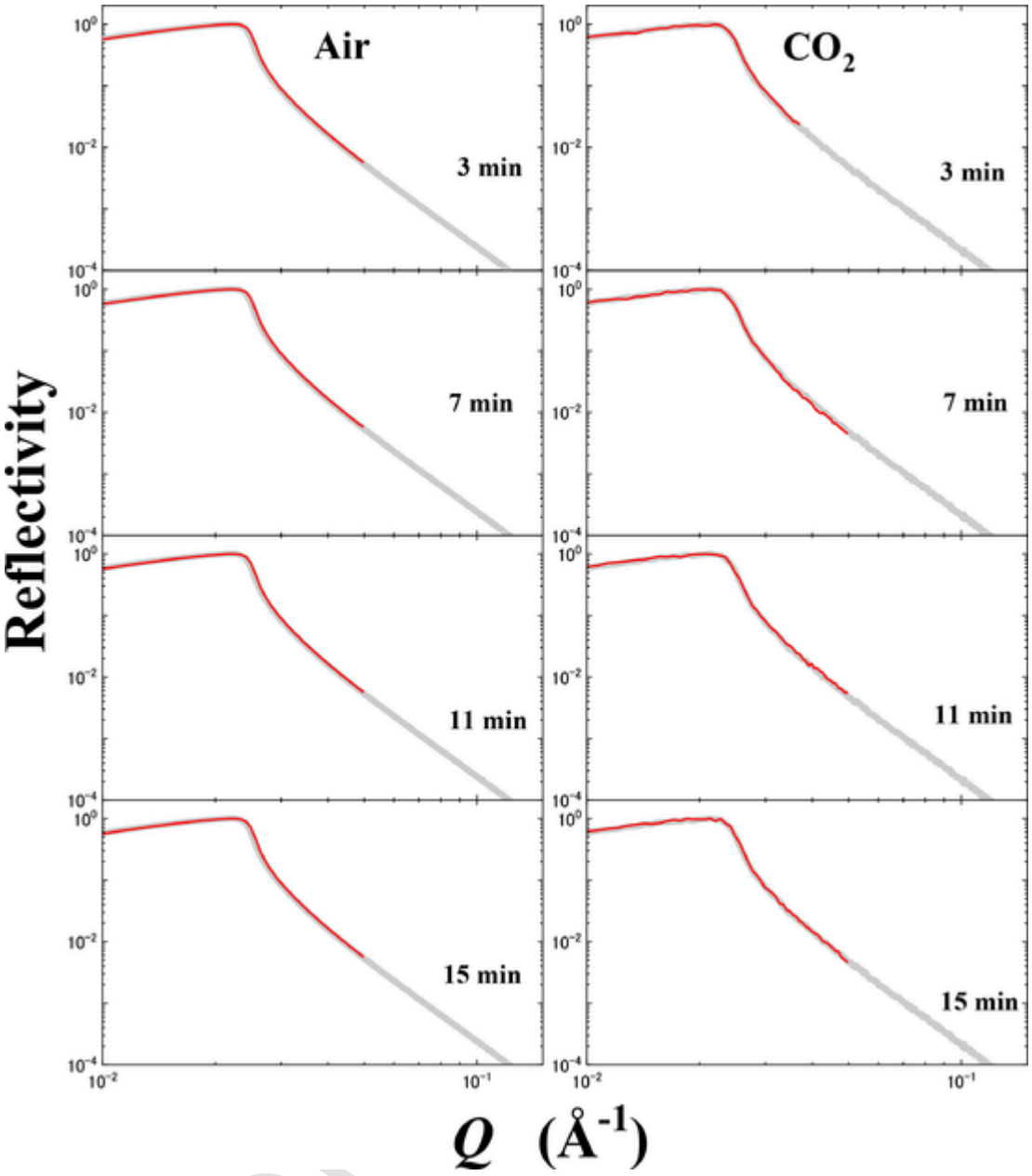

Fig. 4. Time dependence of X-ray reflectivity (XRR) of pure [N4111][TFSI] under air and CO_2. Fully equilibrated XRR is expressed by thick gray curve.

reduction of the 2-propanol Raman band was observed. Even at the bulk state of the 2-propanol-based mixtures, molecular interactions among cation, anion, and 2-propnol did not vary by CO_2. Thus, consistent experimental results indicate that CO_2 enhances the propanol isomer effect in [N3111][TFSI]. The focusing surface density of the 60 mol% propanol, positive $\Delta\rho_m$ was observed in 60 mol% 1- and 2-propanol mixtures. However, both Q_c did not exceed Q_c(pure) of pure [N3111][TFSI] ($\Delta Q_c \leq 0$). In previous study (Abe et al., 2016, 2020), maximum CO_2 capture was observed In the [N3111][TFSI]-60 mol% 2-propanol. Thus, $\Delta\rho_m$ and ΔQ_c of the 60 mol% mixtures are summarized in Table 2. For comparison, two parameters of [N4111][TFSI]-propanol are listed in Table 2, where maximum CO_2 capture occurred at around 70-80 mol% 2-propanol. In case of [N4111][TFSI]-70 mol% 2-propanol (Abe et al., 2020), positive Q_c shifting ($0 < \Delta Q_c$) occurred under CO_2. The positive Q_c shifting exhibits that surface density in the mixture is larger than that in pure [N4111][TFSI] despite propanol dilution. Furthermore, a complementary use of XRR and NR suggests that the specific surface layering exists in [N4111][TFSI]-70 mol% 2-propanol (Abe et al., 2020). The specific surface layering was connected with the high efficiency of CO_2 capture. Therefore, negative ΔQ_c of all [N3111][TFSI]-propanol mixtures is regarded as non-forming specific surface layering. Another significant point is that after XRR experiments, CO_2 bubbles in [N3111][TFSI]-propanol form on the Teflon plate (the bottom side) in the mixed system (Fig. S1). Obviously, the number of bubbles is high in 1-propanol-based mixtures. Similarly, in the case of pure ILs under He conditions, CO_2 in the [N3111][TFSI]-1-propanol could be easily ruled out as an unstable factor. In contrast, no bubbles in [N3111][TFSI]-75.0 mol% 2-propanol indicated that CO_2 is well resolved in the mixture (Fig. S1). Furthermore, negative $\Delta\rho_m$ of [N3111][TFSI]-75.0 mol% 1-propanol and zero $\Delta\rho_m$ of [N3111][TFSI]-75.0 mol% 2-propanol correspond to CO_2 solubility, which is inversely proportional to a number of bubbles.

To clarify the alkyl chain length effect of the surface structures in the [N(n)111][TFSI]-propanol system, XRR of [N6111][TFSI]-propanol was examined (Fig. 6) compared with [N3111][TFSI]-propanol solutions. Here, pure [N6111][TFSI] possessed the largest surface tension,

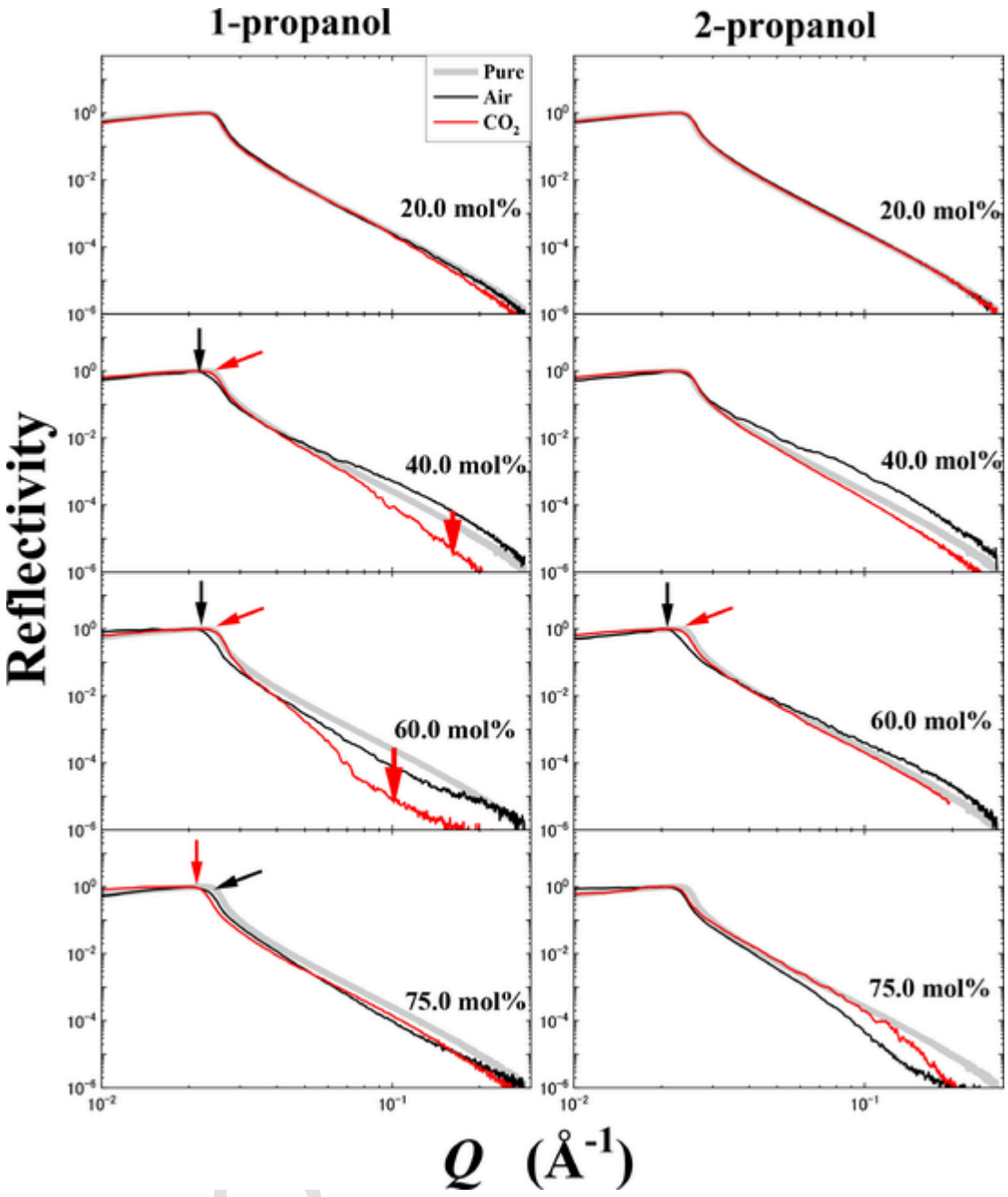

Fig. 5. Equilibrated X-ray reflectivity (XRR) of [N3111][TFSI]-*x* mol% 1-propanol and [N3111][TFSI]-*x* mol% 2-propanol. Red curves indicate XRR under CO_2 (For interpretation of the references to color in this figure legend, the reader is referred to the web version of this article.).

Table 2
The CO_2-enhancement effect ($\Delta\rho_m$) and the mixing effect (ΔQ_c) of [N(*n*)111][TFSI]-1-propanol and -2-propanol.

	[N3111][TFSI] (*x* ~ 60)		[N4111][TFSI] (*x* = 70 ~ 80)		[N6111][TFSI] (*x* ~ 60)	
	1-PrOH	2-PrOH	1-PrOH	2-PrOH	1-PrOH	2-PrOH
$\Delta\rho m$	+	+	~ 0	+	~ 0	~ 0
ΔQc	~ 0	~ 0	-	+	~ 0	~ 0

while surface tension of [N3111][TFSI] is the smallest (Table 1). Below 40 mol%, equilibrated XRR profile of [N6111][TFSI]-propanol solutions almost coincided with XRR of pure [N6111][TFSI] indicated by the thick gray curve (Fig. 6). Under CO_2, a lot of bubbles appeared on the bottom below 40 mol% (Fig. S2). In comparison to the [N3111][TFSI]-propanol system, the number of bubbles in [N6111][TFSI]-2-propanol was greater than that in [N6111][TFSI]-1-propanol. The opposing bubble formation behaviors imply that the propanol isomer effect varies with surface tension. Even at 60 mol%, Q_c did not change in both 1-propanol- and 2-propanol-based mixtures, although XRR(N6, 60, 2, air) profile was modified. Considering maximum CO_2 capture of [N6111][TFSI]-60 mol% 2-propanol (Abe et al., 2020), two parameters are represented in Table 2. [N6111][TFSI]-propanol is characterized by nearly zero $\Delta\rho_m$ and ΔQ_c below 60 mol% (Fig. 6). It is concluded that a rigid surface in [N6111][TFSI]-propanol can be formed, owing to the high surface tension of pure [N6111][TFSI]. In terms of CO_2 capture, very little CO_2 capture was achieved in [N6111][TFSI]-propanol (Abe et al., 2020). Surface reconstruction for the specific surface layering did not occur due to non-variable XRR in [N6111][TFSI]-propanol.

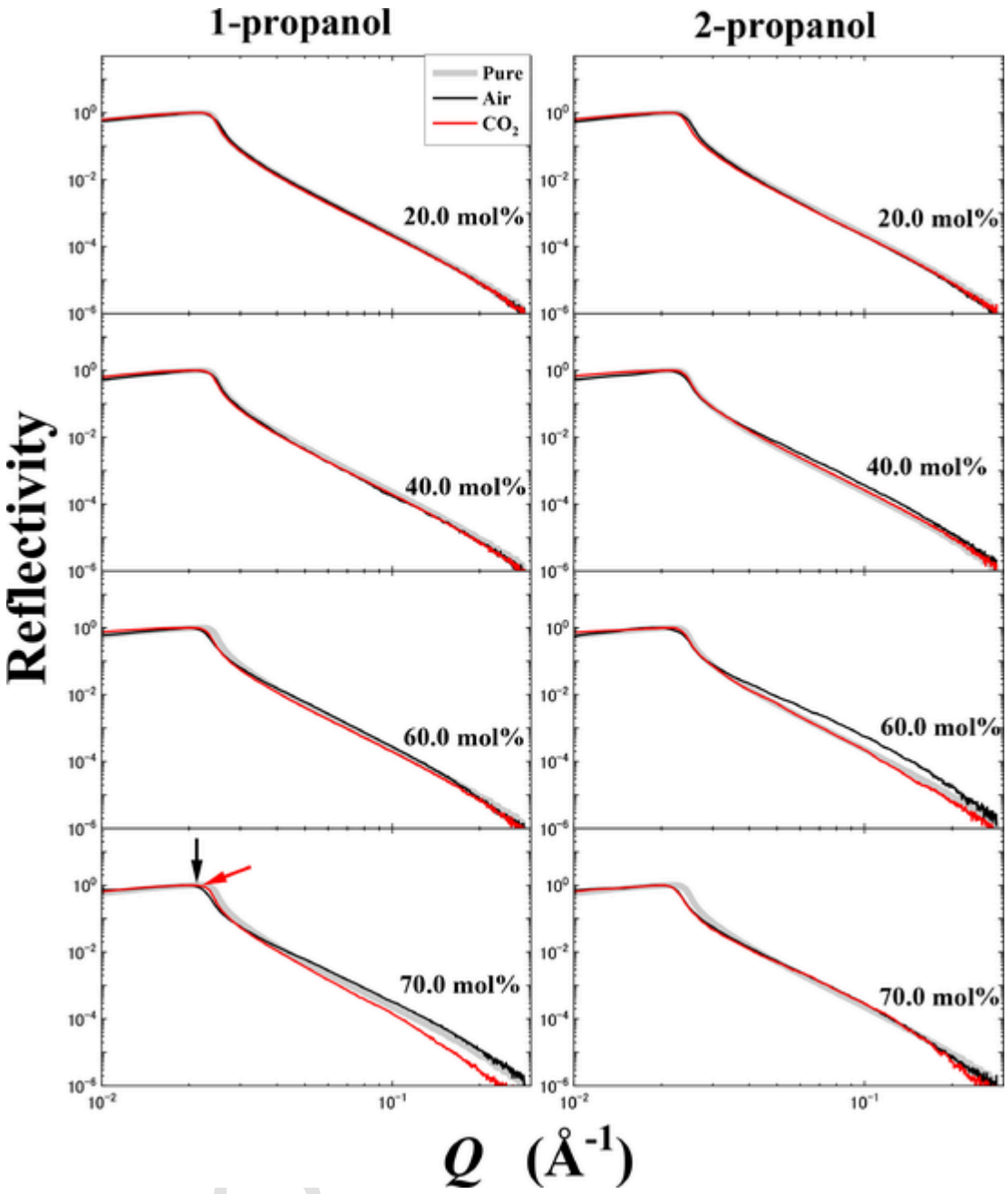

Fig. 6. Equilibrated X-ray reflectivity (XRR) of [N6111][TFSI]-*x* mol% 1-propanol and [N6111][TFSI]-*x* mol% 2-propanol. Red curves indicate XRR under CO_2 (For interpretation of the references to color in this figure legend, the reader is referred to the web version of this article.).

3.3. Kinetic behaviors of X-ray reflectivity in quaternary ammonium ionic liquid-propanol solutions

Combined with CO_2 capture abilities in [N(*n*)111][TFSI]-propanol, characteristic features of equilibrated surface structures are distinguished as listed in Table 2. CO_2 enhancement effect ($\Delta\rho_m$) and mixing effect (ΔQ_c) parameters are indispensable for further understanding. Two positive parameters of [N4111][TFSI]-2-propanol imply that the surface enrichment is caused to stabilize the surface state. After stabilization, the specific surface layering corresponds to high efficiency for CO_2 capture. To interpret surface reconstruction related to the CO_2 absorption process, time-resolved XRR experiments were carried out. Fig. 7 reveals the time dependence of XRR in [N3111][TFSI]-60.0 mol% 1-propanol, where the thick gray curves in the figure represent XRR of pure [N3111][TFSI] for a comparison. Under the air, a gradual Q_c shift to a higher Q position was observed with the lapse of time. Contrary to the pure time-invariant system (Fig. 4), the surface structure obtained by XRR(N3, 60, 1, air) depended obviously on time. Moreover, the fluctuated XRR of [N3111][TFSI]-60.0 mol% 1-propanol was enhanced under CO_2 (Fig. 7). For instance, at the early stage of CO_2 capture, the Q_c position under CO_2 is lower than that under the air. Also, profile oscillations of XRR(N3, 60, 1, CO_2) on the Q scale were distinct. Therefore, CO_2 could disturb the surface flatness of [N3111][TFSI]-60.0 mol% 1-propanol, and lowered the surface density at the early stage. On the contrary, at the late stage, Q_c was shifting to a higher position but did not exceed Q_c of pure [N3111][TFSI] ($\Delta Q_c \sim 0$). Therefore, the equilibrated surface state became stable, but the specific surface layering was not formed in [N3111][TFSI]-1-propanol.

More importantly, remarkable surface instability under CO_2 was observed at the early stage of the 2-propanol-based mixtures. For instance,

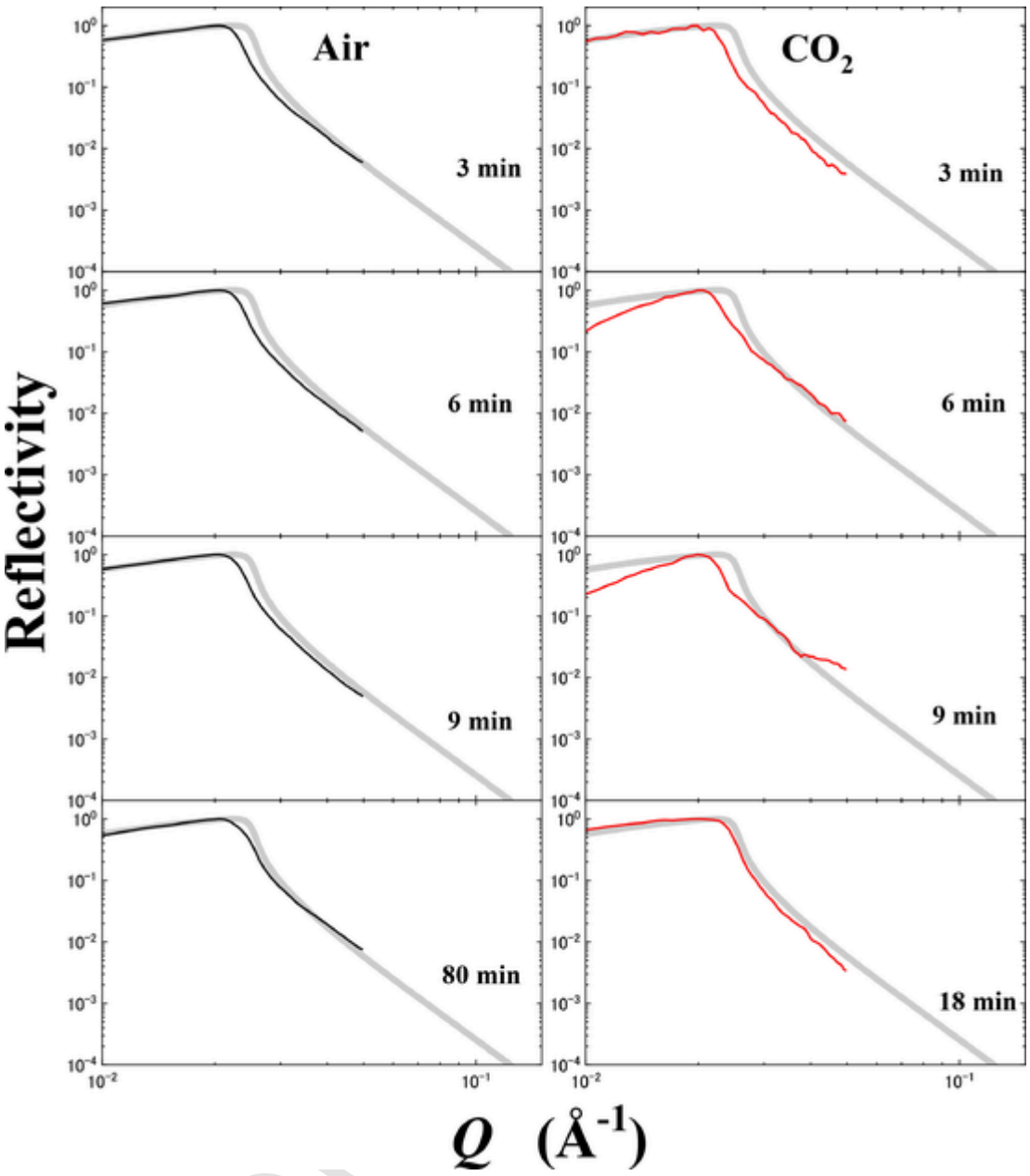

Fig. 7. Time-resolved X-ray reflectivity of [N3111][TFSI]-60.0 mol% 1-propanol.

[N3111][TFSI]-60.0 mol% 2-propanol provided time- and *Q*-sensitive XRR under CO_2 (Fig. 8). Compared to the 1-propanol-based mixture under CO_2 (Fig. 7), the surface state of the mixture with 2-propanol and CO_2 is more unstable. Surface roughness is caused by 2-propanol coupled with CO_2 on the surface, representing the energetically unstable surface. However, within 26 min, the unstable surface at the early stage of XRR(N3, 60, 2, CO_2) drastically changed to the equilibrated XRR. In addition to oscillating XRR extensively for 6 min, Q_c located the lower *Q* position for the first 6 min. At the early stage, the low-density state could promote the molecular exchange near the surface. After surface reconstruction, the surface state became stable, accompanying large surface density. In contrast, XRR(N3, 60, 2, air) did not fluctuate extensively. Under the air, the CO_2-enhanced fluctuations were much suppressed (Fig. 8). Under the air, surface improvement was not induced because of low surface density ($\Delta Q_c < 0$) and little fluctuations of XRR (N3, 60, 2, air).

Specific surface layering is a key to interpret high efficiency of CO_2 capture in [N4111][TFSI]-2-propanol, satisfying with positive $\Delta\rho_m$ and ΔQ_c (Table 2). *In-situ* observation of XRR can extract hidden information about the formation process of the specific surface layering. At first, time-evolution of XRR in [N4111][TFSI]-75.0 mol% 1-propanol is revealed in Fig. S3. Time-steady XRR(N4, 75, 1, air) profiles were observed. A stable surface was formed under the air, although surface density was low. Even under CO_2, Q_c of the 1-propanol-based mixture shifted a little at the early stage. Non-oscillated XRR(N4, 75, 1, CO_2) indicated that CO_2-driven instability is not induced. Next, the 2-propanol effect for the formation process of the surface layering was examined. [N4111][TFSI]-75.0 mol% 2-propanol indicated small time changes of XRR under air (Fig. S4). XRR profiles fluctuated little at around 9 min. During 17 min measurements, the Q_c position of XRR(N4, 75, 2, air) was almost constant. Also, negative ΔQ_c means that, under the air, the surface density of the 2-propanol mixture is small. Hence, under the air, the surface state of [N4111][TFSI]-75.0 mol% 2-propanol was stable with low surface density. However, under CO_2, XRR(N4, 75, 2, CO_2) was drastically changed (Fig. S4). Relative large fluctuation of XRR was observed at 5 min. Even at an early stage of CO_2 capture, ΔQ_c was al-

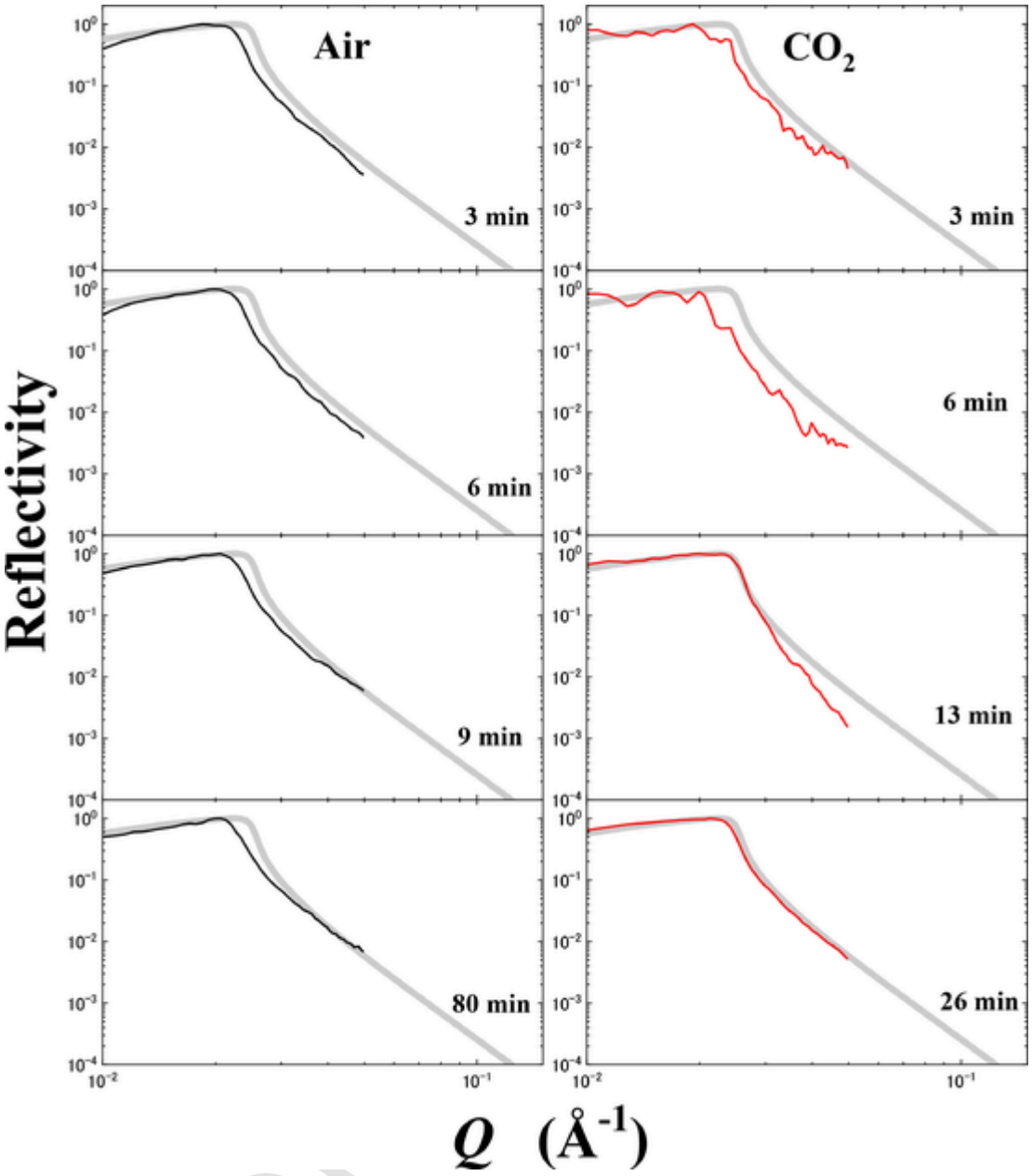

Fig. 8. Time-resolved X-ray reflectivity of [N3111][TFSI]-60.0 mol% 2-propanol.

most nearly zero. Compared with Q_c under the air, $\Delta\rho_m$ was positive distinctly. Particularly under CO_2, high surface density ($\Delta Q_c \sim 0$) even in the 2-propanol-diluted mixture suggests that CO_2 is involved in the surface layer, and the molecular rearrangement occurred in the high surface density circumstance until 5 min. By a complementary use of XRR and NR (Abe et al., 2020), the surface layer model was provided by introducing the specific $[TFSI]^-$ anion and CO_2 layer. Formation of the specific surface layering was interpreted by time dependences of the CO_2 molar fraction, η, of [N4111][TFSI]-80.5 mol% 2-propanol (Abe et al., 2020). Only in [N4111][TFSI]-2-propanol, two steps in the CO_2 absorption process appeared. The first slow CO_2 absorption finished at 220 s ($\eta \sim 5$ mol%). After that, a rapid increase η occurred. Here, it is deduced that the specific layer could be formed gradually during the first step of CO_2 capture. After stopping the CO_2 supply, a slow mass decay appeared below 5 mol%. Therefore, the specific surface layering ($[TFSI]^-$ and CO_2) having high surface density could be rigid. With passing time, Q_c of XRR(N4, 75, 2, CO_2) was shifting to a higher position. At the late stage of CO_2 capture, increment of the surface density implies that more than 5 mol% CO_2 contributed to the specific surface layering. Time dependence of XRR and CO_2 mass transfer were consistent and can explain the specific surface layering formation.

Time-resolved XRR of [N6111][TFSI]-60.0 mol% 1-propanol was measured to clarify the alkyl chain length effect. XRR(N6, 60, 1, air) was time-invariant (Fig. S5). While, XRR(N6, 60, 1, CO_2) indicated the Q_c shifting and a little fluctuation of XRR at 6 min. More importantly, drastic time changes of XRR occurred in the 2-propanol-based mixtures. The kinetic fluctuations of XRR profiles were discovered to be caused by unstable surface layers. For example, [N6111][TFSI]-60.0 mol% 2-propanol in the air provided almost constant XRR oscillations and Q_c (Fig. S6). Further XRR profile fluctuations appeared in the presence of CO_2. Surface instabilities were more pronounced in time-resolved XRR (N6, 60, 2, CO_2) under CO_2. At the early stage of the CO_2 capture process, negative ΔQ_c and the distinct fluctuations of the XRR profiles were similar to time-resolved XRR(N3, 60, 2, CO_2) (Fig. 8). In the same manner with the [N3111][TFSI]-2-propanol under CO_2, ΔQ_c on the XRR(N6, 60, 2, CO_2) became nearly zero at the late stage. Also, in

[N6111][TFSI]-2-propanol, CO_2-mediated molecular exchanges occur, and the surface state was stabilized by the high surface density ($0 < \Delta\rho_m$).

4. Conclusions

In-situ observations of XRR profiles under a CO_2 atmosphere were carried out on pure [N(*n*)111][TFSI], [N(*n*)111][TFSI]-1-propanol and [N(*n*)111][TFSI]-2-propanol systems. In a pure [N(*n*)111][TFSI] system, stable surface structures were formed under any gas atmosphere. In the mixed system, characteristic $\Delta\rho_m$ as CO_2-enhancement effect and ΔQ_c as mixing effect were obtained from the equilibrated XRR. Positive values both of $\Delta\rho_m$ and ΔQ_c are required for the specific surface layering to obtain high CO_2 capture in [N(*n*)111][TFSI]-propanol. Time-resolved XRR examined the surface reconstruction process. The fluctuated XRR profile and low surface density at the early stage of CO_2 absorption, particularly in 2-propanol-based mixtures, suggested that 2-propanol induces an energetically unstable surface state on the surface and surface fluctuations are accelerated under CO_2. The molecular rearrangement took place near the surface to find a stable surface state. Once the distinct XRR oscillation finished, Q_c shifted to a higher Q position. The optimized surface structure in [N4111][TFSI]-2-propanol under CO_2 is regarded as the specific surface layering. The CO_2-assisted densely packed surface layering contributes to high efficiency for CO_2 capture in [N4111][TFSI]-2-propanol.

Declaration of Competing Interest

There are no conflicts to declare.

Acknowledgements

We appreciate Dr. F. Nemoto, Dr. S. Shimono, Dr. T. Takekiyo and Prof. Y. Yoshimura of National Defense Academy for helpful discussions.

Supplementary materials

Supplementary material associated with this article can be found, in the online version, at doi:10.1016/j.jil.2022.100018.

References

Rosa, L., Reimer, J.A., Went, M.S., D'Odorico, P., 2020. Hydrological limits to carbon capture and storage. Nat. Sustain. 3, 658–666.
Schoedel, A., Ji, Z., Yaghi, O.M., 2016. The role of metal-organic frameworks in a carbon-neutral energy cycle. Nat. Energy 1, 16034, -13.
Hepburn, C., Adlen, E., Beddington, J., Carter, E.A., Fuss, S., Dowell, N.Mac, Minx, J.C., Smith, P., Williams, C.K., 2019. The technological and economic prospects for CO_2 utilization and removal. Nature 575, 87–97.
Blanchard, L.A., Hancu, D., Beckman, E.J., Brennecke, J.F., 1999. Green processing using ionic liquids and CO_2. Nature 399, 28–29.
Bara, J.E., Carlisle, T.K., Gabriel, C.J., Camper, D., Finotello, A., Gin, D.L., Noble, R.D., 2009. Guide to CO_2 separations in Imidazolium-based room-temperature ionic liquids. Ind. Eng. Chem. Res. 48, 2739–2751.
Brennecke, J.F., Gurkan, B.E., 2010. Ionic Liquids for CO_2 capture and emission reduction. J. Phys. Chem. Lett. 1, 3459–3464.
Ramdin, M., de Loos, T.W., Vlugt, T.J.H., 2012. State-of-the-art of CO_2 capture with ionic liquids. Ind. Eng. Chem. Res. 51, 8149–8177.
Zeng, S., Zhang, X., Bai, L., Zhang, X., Wang, H., Wang, J., Bao, D., Li, M., Liu, X., Zhang, S., 2017. Ionic-liquid-based CO_2 capture systems: structure, interaction and process. Chem. Rev. 117, 9625–9673.
Zhai, H., Rubin, E.S., 2017. Technical and economic assessments of ionic liquids for precombustion CO_2 capture at IGCC power plants. Energy Proced. 114, 2166–2172.
Mota-Martinez, M.T., Brandl, P., Hallett, J.P., Dowell, N.M., 2018. Challenges and opportunities for the utilisation of ionic liquids as solvents for CO_2 capture. Mol. Syst. Des. Eng. 3, 560–571.
Tang, J., Tang, H., Sun, W., Plancher, H., Radosz, M., Shen, Y., 2005. Poly(ionic liquid)s: a new material with enhanced and fast CO_2 absorption. Chem. Commun. 3325–3327.
Abe, H., Takeshita, A., Sudo, H., Akiyama, K., Kishimura, H., 2016. CO_2 capture at room temperature and ambient pressure: isomer effect in room temperature ionic liquid/propanol solutions. Green Sustain. Chem. 6, 116–124.
Abe, H., Nemoto, F., Kishimura, H., Ozawa, S., 2020. CO_2 capture by quenched quaternary ammonium ionic liquid-propanol mixtures assessed by Raman spectroscopy. J. Mol. Liq. 315, 113687–113688.
Su, T., Tang, Z., Yin, C., Yang, Y., Wang, H., Peng, L., Su, Y., Su, P., Li, J., 2021. Insights into quaternary ammonium-based ionic liquids series with tetrafluoroborate anion for CO_2 capture. J. Mol. Liq. 327, 114857, -10.
Carmichael, A.J., Hardacre, C., Holbrey, J.D., Nieuwenhuyzen, M., Seddon, K.R., 2001. Molecular layering and local order in thin films of 1-alkyl-3-methylimidazolium ionic liquids using X-ray reflectivity. Mol. Phys. 99, 795–800.
Solutskin, E., Ocko, B.M., Taman, L., Kuzmenko, I., Gog, T., Deutsch, M., 2005. Surface layering in ionic liquids: an X-ray reflectivity study. J. Am. Chem. Soc. 127, 7796–7804.
Sloutskin, E., Lynden-Bell, R.M., Balasubramanian, S., Deutscha, M., 2006. The surface structure of ionic liquids: comparing simulations with x-ray measurements. J. Chem. Phys. 125, 174715–174717.
Mezgera, M., Ockoc, B.M., Reichertd, H., Deutsche, M., 2013. Surface layering and melting in an ionic liquid studied by resonant soft X-ray reflectivity. Proc. Natl. Acad. Sci. 110, 3733–3737.
Yan, T., Li, S., Jiang, W., Gao, X., Xiang, B., Voth, G.A., 2006. Structure of the liquid-vacuum interface of room-temperature ionic liquids: a molecular dynamics study. J. Phys. Chem. B 110, 1800–1806.
Shimizu, K., Heller, B.S.J., Maier, F., Steinrück, H.P., Canongia Lopes, J.N., 2018. Probing the surface tension of ionic liquids using the langmuir principle. Langmuir 34, 4408–4416.
Lauw, Y., Horne, M.D., Rodopoulos, T., Lockett, V., Akgun, B., Hamilton, W.A., Nelson, A.R.J., 2012. Structure of $[C_4mpyr][NTf_2]$ room-temperature ionic liquid at charged gold interfaces. Langmuir 28, 7374–7381.
Abe, H., Takeshita, A., Sudo, H., Akiyama, K., 2020. CO_2 capture and surface structures of ionic liquid-propanol solutions. J. Mol. Liq. 301, 112445–112447.
Abe, H., Murata, K., Kiyokawa, S., Yoshimura, Y., 2018. Surface tension anomalies in room temperature ionic liquids-acetone solutions. Chem. Phys. Lett. 699, 275–278.
Nemoto, F., Nakamura, S., Abe, H., 2021. Surface structure of the mixture of 1-alkyl-3-methylimidazolium iodide and polyiodide observed by surface tension measurement and X-ray reflectivity. J. Mol. Liq. 337, 116381–116386.
Matsumoto, H., Yanagida, M., Tanimoto, K., Nomura, M., Kitagawa, Y., Miyazaki, Y., 2000. Highly conductive room temperature molten salts based on small trimethylalkylammonium cations and bis(trifluoromethylsulfonyl)imide. Chem. Lett. 8, 922–923.
Zhang, S., Sun, N., He, X., Lu, X., Zhang, X., 2006. Physical properties of ionic liquids: database and evaluation. J. Phys. Chem. Ref. Data 35, 1475–1517.
Chau, J., Obuskovic, G., Jie, X., Mulukutla, T., Sirkar, K.K., 2013. Solubilities of CO_2 and helium in an ionic liquid containing poly(amidoamine) dendrimer Gen 0. Ind. Eng. Chem. Res. 52, 10484–10494.
Veldhuis, S.A., Brinks, P., Stawski, T.M., Göbel, O.F., ten Elshof, J.E., 2014. A facile method for the density determination of ceramic thin films using X-ray reflectivity. J. Sol-Gel Sci. Technol. 71, 118–128.
Tidswell, I.M., Ocko, B.M., Pershan, P.S., Wasserman, S.R., Whitesides, G.M., Axe, J.D., 1990. X-ray specular reflection studies of silicon coated by organic monolayers (alkylsiloxanes). Phys. Rev. B 41, 1111–1128.
Braslau, A., Deutsch, M., Pershan, P.S., Weiss, A.H., Als-Nielsen, J., Bohr, J., 1985. Surface roughness of water measured by X-ray reflectivity. Phys. Rev. Lett. 54, 114–117.
Naeiji, P., Woo, T.K., Alavi, S., Ohmura, R., 2020. Molecular dynamics simulations of interfacial properties of the CO_2–water and CO_2–CH_4–water systems. J. Chem. Phys. 153, 044701–044713.